catalysts

MDPI

Communication

A DFT Investigation on the Origins of Solvent-Dependent Polysulfide Reduction Mechanism in Rechargeable Li-S Batteries

Guan-Ying Du, Chi-You Liu and Elise Y. Li *

Department of Chemistry, National Taiwan Normal University No. 88, Section 4, Tingchow Road, Taipei 116, Taiwan; candlelights999@gmail.com (G.-Y.D.); 80542002S@ntnu.edu.tw (C.-Y.L.)

* Correspondence: eliseytli@ntnu.edu.tw; Tel.: +886-2-77496219; Fax: +886-2-29324249

Received: 14 May 2020; Accepted: 4 August 2020; Published: 10 August 2020

Abstract: The lithium-sulfur (Li-S) battery is one of the promising energy storage alternatives because of its high theoretical capacity and energy density. Factors governing the stability of polysulfide intermediates in Li-S batteries are complex and are strongly affected by the solvent used. Herein, the polysulfide reduction and the bond cleavage reactions are calculated in different solvent environments by the density functional theory (DFT) methods. We investigate the relationship between the donor numbers (DN) as well as the dielectric constants (ε) of the solvent system and the relative stability of different polysulfide intermediates. Our results show that the polysulfide reduction mechanism is dominated by its tendency to form the ion-pair with Li^+ in different organic solvents.

Keywords: Li-S battery; donor number; dielectric constant; polysulfides; solvent effect; DFT

1. Introduction

Lithium-sulfur (Li-S) batteries, with their high theoretical energy density of 2600 Wh/kg, are attracting much attention as future energy storage systems in various fields, including portable electronic devices, hybrid to full electric vehicles (EVs), and large-scale power grids [1,2]. Since the sulfur cathode could undergo multiple electron transfer events during the Li-S battery operations, a high theoretical capacity (1675 mAh/g) can be achieved. In comparison, the conventional intercalated $LiCoO_2$ cathode in the lithium-ion batteries (LIB) shows a capacity of around only 140 mAh/g [3]. The abundant quantity and the low cost of the sulfur resources on earth also guarantee economic advantages of Li-S batteries [4–6]. Overall, the predicted high efficiency and the environmental compatibility of the Li-S batteries have made them the most promising candidate to overcome the intrinsic limitation of the common batteries for the next generation rechargeable energy storage system [4,7–9].

However, the development on the application of Li-S batteries is hindered by various problems, including the shuttle effect [9–12] and the dendrite formation at the anode [13,14], etc. The combined effects of the physical properties, such as viscosity, conductivity, and safety issues of the electrolyte system [15,16], the salt additives [17], electrode materials [18–21], interface stabilities [22–25], etc., have been the subject of intense investigations in the past decade aiming for the practical and sustainable scaling of high-performance Li-S batteries [26,27]. The physical environment of a Li-S battery is an extremely complicated system and the plethora of experimental attempts are still largely based on trial and error. Large-scale theoretical simulations have also been carried out to improve the fundamental understanding of the structural and transport behaviors of the intermediates, the interaction between the electrolyte and the reacting species, and the adsorption event at the electrode surfaces [28–33].

In principle, the selection of the solvent and the electrolyte system is critical to the battery performance since the sulfur reduction mechanisms [10,34–36] depend strongly on the dissolution,

diffusion and disproportionation reactions of soluble polysulfides in the solvent environment [5,9,37–44]. The chain length distribution of the polysulfide species intimately affects the diffusion coefficients, the conductivities, clustering, and even the extent of the shuttle effect [12,28,29]. Meanwhile, the major polysulfide species may exist in different forms [44] depending on the solvent system [38,43,45], the ionic additives [46], and even the concentrations [43]. For example, a previous study has shown that different alkali-metal cations could stabilize polysulfides of different length, e.g., S_4^{2-} or S_3^{2-} [38]. It was also observed that the radical polysulfide species are favored at lower sulfur concentrations, while the doubly charged, dimerized polysulfide species are favored at higher sulfur concentrations [43] in accordance with chemical equilibrium. For the more fundamental solvent effect, different theories have been suggested to rationalize experimental observations. For example, the most stable polysulfide intermediate may exist as S_3^- radicals in dimethyl sulfoxide (DMSO), or as S_4^{2-} in the mixed solvent system, 1,3-dioxane:1,2-dimethoxyethane (DOL:DME) [38,47]. A different study reported that polysulfide radicals (i.e., S_4^-) can be selectively stabilized in ether-based electrolytes, such as in tetraethylene glycol dimethyl ether (TEGDME), and polyethylene oxide (PEO) [43,48]. These phenomena were tentatively correlated with the dielectric constant (ε) and/or the donor number (DN) of the solvent system. Nevertheless, a microscopic understanding is lacking. In general, the ε of the solvent is related to the stability of polar or ionic solute species, and the DN is directly related to the complexation between the cation and the solvent molecules. Therefore, a single parameter may not offer a comprehensive explanation to the observed tendency of the dominant polysulfide species. A more profound understanding of the multiple polysulfide reduction pathways in different electrolytes is necessary.

In this work, we focus on the interaction between polysulfides, lithium ions, and the solvent system. The structures of the polysulfides and the lithium polysulfides (LiPSs) in different solvent systems are simulated, and various possible reduction pathways of these species are characterized. We consider both the implicit solvent model and the explicit solvent binding with Li^+. Our results shall help establish the dominant factors of polysulfide stabilities, which may be applied to solvent system optimization in Li-S battery design.

2. Results and Discussions

The optimized geometries of polysulfides (PS) and lithium polysulfides (LiPS) in DMSO are shown in Supplementary Figure S1 and Figure 1, respectively. Note that the overall geometries are similar in different solvents. The lengths of S-S bonds are in the range of 1.99 to 2.19 Å for both PS's and LiPS's, and the lengths of Li-S bonds are in the range of 2.37 to 2.44 Å. The overall geometry and the detailed geometry parameters are consistent with previously reported values [29,33,49–51]. We then consider the electrochemistry profile and compute the reduction potentials for major polysulfide reduction reactions, as shown in Supplementary Table S1. Note that since the mixed-solvent system DOL:DME cannot be easily simulated by the implicit solvent model, we adopt the THF solvent system which has a similar molecular motif and dielectric constant ($\varepsilon_{\mathbf{THF}} = 7.43$) value with DOL and DME ($\varepsilon_{DOL} = 7.3$ and $\varepsilon_{DME} = 7.2$). As can be expected, the calculated reduction potentials increase in solvents with higher dielectric constant as the anions are stabilized in polar solvents. Overall, the computed theoretical values are consistent with the cyclic voltammogram experimental values.

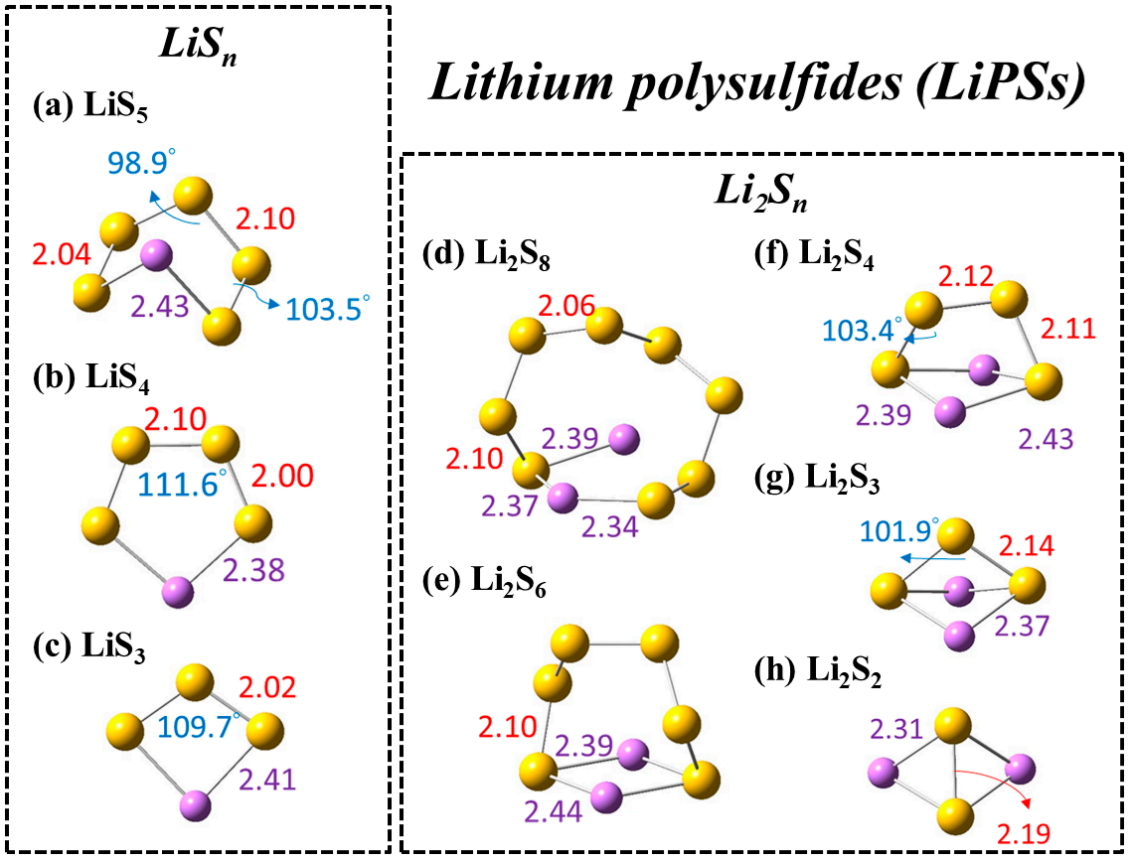

Figure 1. Optimized geometries of different LiPSs in DMSO. The average bond lengths of S-S (d, in Å) and the bond angles (θ, in °) are labeled in red and purple, respectively.

2.1. Solvent-Dependent PS Reaction Pathways

To further explore the reactions of PS in different solvents, we consider some possible reaction pathways (Reactions (1)–(8) in Table 1) based on the results from UV-Vis spectroscopy [38,52,53], and we calculate their reaction free energies (ΔG). In solvents with medium to low polarity ($\varepsilon < 10$), it has been proposed that the PS species may exist as neutral lithium polysulfides (LiPS) [44]. Therefore, the aforementioned reaction pathways between the undissociated LiPS reactants are also considered as Reactions (9)–(16) in Table 2.

Table 1. The reaction free energies (ΔG, eV) of polysulfides in different solvents. The dielectric constants (ε) of different solvents are presented in parentheses. The solvents that tend to facilitate the reactions of the dissociated PS's are shaded in grey, and the reaction energies for the more probable reactions are in bold.

#	Reactions	DIOX (2.21)	THF (7.43)	Acetone (20.49)	ACN (35.69)	DMSO (46.83)
1	$S_8^{2-} \rightarrow S_6^{2-} + S_2$	0.47	0.38	**0.31**	**0.32**	**0.32**
2	$S_8^{2-} \rightarrow S_5^{-} + S_3^{-}$	−0.87	−0.08	**0.16**	**0.23**	**0.26**
3	$S_8^{2-} \rightarrow S_4^{2-} + S_4$	1.63	1.25	1.12	1.11	1.11
4	$S_8^{2-} \rightarrow 2S_4^{-}$	−0.76	0.04	**0.23**	**0.29**	**0.31**
5	$S_6^{2-} \rightarrow 2S_3^{-}$	−1.30	−0.45	**−0.19**	**−0.12**	**−0.10**
6	$S_6^{2-} \rightarrow S_4^{2-} + S_2$	0.98	0.70	0.63	0.62	0.62
7	$2S_4^{2-} \rightarrow 2S_3^{-} + S_2^{2-}$	−0.27	0.39	0.60	0.66	0.69
8	$2S_4^{2-} \rightarrow S_6^{2-} + S_2^{2-}$	1.03	0.84	0.80	0.78	0.78

Table 2. The reaction free energies (ΔG, eV) of lithium polysulfides in different solvents. The dielectric constants (ε) of different solvents are presented in parentheses. The solvents that tend to facilitate the reactions of the bound LiPS's are shaded in grey, and the reaction energies for the more probable reactions are in bold.

#	Reactions	DIOX (2.21)	THF (7.43)	Acetone (20.49)	ACN (35.69)	DMSO (46.83)
9	$Li_2S_8 \rightarrow Li_2S_6 + S_2$	**0.20**	**0.19**	**0.17**	0.18	0.19
10	$Li_2S_8 \rightarrow LiS_5 + LiS_3$	1.13	0.95	0.85	0.80	0.91
11	$Li_2S_8 \rightarrow Li_2S_4 + S_4$	0.85	0.81	0.79	0.79	0.81
12	$Li_2S_8 \rightarrow 2LiS_4$	1.15	0.97	0.89	0.87	0.87
13	$Li_2S_6 \rightarrow 2LiS_3$	0.88	0.67	0.57	0.48	0.70
14	$Li_2S_6 \rightarrow Li_2S_4 + S_2$	**0.47**	**0.45**	**0.44**	0.45	0.46
15	$2Li_2S_4 \rightarrow 2LiS_3 + Li_2S_2$	2.11	1.71	1.37	1.21	1.12
16	$2Li_2S_4 \rightarrow Li_2S_6 + Li_2S_2$	0.97	0.82	0.70	0.65	0.64

The absorption spectrum of the PS's in DMSO indicates the existence of the species S_8^{2-}, S_6^{2-}, S_4^{2-}, and S_3^- [11]. In contrast, the reactions between sulfur and various lithium polysulfides in DOL:DME (represented by THF in our theoretical simulation) mainly produce the species S_8^{2-} and S_4^{2-} [38]. Therefore, for the initial S_8^{2-} decomposition step, several crucial reactions are considered as shown by Reactions (1)–(4). Although the neutral cyclic S_5 molecules and the radical anions S_5^- have not been experimentally observed in solution or in the solid state [44], their existence cannot be completely ruled out and are therefore considered as the decomposition product within the first few steps (Reaction (2)). Further decompositions of the short-chain PS species (S_6^{2-}) are proposed to proceed by Reactions (5) and (6). The origins of the observed species may also come from disproportionation reactions such as Reactions (7) and (8). In general, for the same reaction, the reaction Gibbs free energy may monotonously decrease (Reactions (1) and (3)), or increase (Reactions (2) and (4)) with increasing solvent dielectric constant (ε) from DIOX to DMSO. Reaction (3) may be ruled out based on its high endothermicity (ΔG > 1.10 eV) in all solvent systems.

For solvents with a high dielectric constant, the polysulfide intermediates are expected to exist as dissociated ionic species. For example, in the DMSO, the reaction energies of three considered decomposition reactions of S_8^{2-} (Reactions (1), (2), and (4)) are all slightly endothermic (ΔG ~ 0.3 eV), and are all likely to proceed. The existence of the decomposed products S_6^{2-} (Reaction (1)) and S_3^- (Reaction (2)) have been observed experimentally [38]. The S_6^{2-} may also easily undergo a bond cleavage to form two S_3^- radical anions, as shown by the slightly exothermic Reaction (5). In comparison, the decomposition of S_6^{2-} to form S_4^{2-} (Reaction (6)) involves a higher reaction energy (0.62 eV) and its occurrence is deemed more unlikely. The experimentally [11] observed S_4^{2-} may result from the reduction of the S_4^- product in Reaction (4). Similarly, the relatively higher reaction Gibbs free energies involved in the disproportionation reactions in Reactions (7) and (8) have rendered these pathways rather improbable.

Unlike the reactions between the ionic species as in Table 1, the ΔG's for neutral reactants are much less dependent on the ε, as the numerical values of the ΔG's for the same reaction are all relatively similar in different solvents in Table 2. In solvents with low ε, e.g., DIOX or THF, the polysulfide intermediates are expected to exist as the neutral bound LiPS species. For these systems, the results indicate that the more probable decomposition pathways are Reaction (9) followed by Reaction (14), in which the Li_2S_8 species first decompose into Li_2S_6, and then to Li_2S_4. Recall that the major species observed in DOL:DME are S_8^{2-} and S_4^{2-} [38], which is consistent with our calculation results. Other reaction pathways generating the LiS_3 (Reactions (10), (13), and (15) in Table 2) are deemed less probable due to their high endothermic characters (ΔG > 0.5 eV).

2.2. The Effect of Solvent Donor Number (DN)

In a few cases, it has been observed that a high dielectric solvent may also facilitate the reaction pathway of the LiPS rather than the dissociated PS [38]. It has been proposed that, other than the

dielectric constant, the donor number (DN) is another important factor governing solvent reactions. The donor number, defined as the negative enthalpy value for the 1:1 adduct formation in the dilute solution of a Lewis base and the standard Lewis acid antimony pentachloride ($SbCl_5$) in the non-coordinating solvent 1,2-dichloroethane [54], is a parameter describing the cation coordinating power of solvents. To quantify the effect of the DN, we calculate the average binding energies ($\overline{E_b}$) for three high dielectric solvent systems, with moderate to high donor numbers. The estimated coordination numbers and the optimized geometries are shown in Table 3 and Supplementary Figure S2, respectively. The cutoff binding energy for the predicted maximal coordination number (n_p) is set as −0.30 eV based on the experimental observation of $[Li\text{-}(DMSO)_4]^+$ [46]. As can be expected, the value of n_p increases with the DN. The calculated small coordination number for Li^+ in ACN (n_p = 2) indicates that the Li^+ cations are less solvated in ACN than the solvents with higher DN, such as in DMSO (n_p = 4). In other words, the more unshielded Li^+ cations in ACN may lead to a stronger attraction to the PS anions. As a result, the chemical equilibrium is expected to shift towards the bound LiPS ion pairs and their respective reaction pathways. This could explain the experimental observation that ACN, despite its intrinsic high dielectric constant (ε = 35.69), behaves like DOL:DME with dominant species S_8^{2-} and S_4^{2-}, or more accurately, the Li_2S_8 and Li_2S_4 [55].

Table 3. The predicted coordination number (n_p) as well as the average binding energies ($\overline{E_b}$) with different number of binding solvent molecules (n) on Li^+ cation. The donor number (DN) and the dielectric constants (ε) of different solvents are also listed.

Solvent	DN	ε	n_p	$\overline{E_b}$			
				n = 1	n = 2	n = 3	n = 4
ACN	14.1	35.69	2	−0.40	−0.35	−0.29	−0.22
Acetone	17.0	20.49	3	−0.51	−0.45	−0.31	−0.25
DMSO	29.8	46.83	4	−0.77	−0.67	−0.52	−0.40

3. Computational Details

Density functional theory (DFT) calculations of molecules are performed by the Gaussian 09 program [56]. The geometries of polysulfides, lithium polysulfides, solvent molecules and $[Li\text{-}(solvent)_n]^+$ (n = 1–4) are calculated at the UM11/6 − 311 + G** level [57]. The implicit SMD [58] continuous solvation model is applied to simulate the five selected solvent environments with different dielectric constants (ε), including 1,4-dioxane (DIOX, ε = 2.21), tetrahydrofuran (THF, ε = 7.43), acetone (ε = 20.49), acetonitrile (ACN, ε = 35.69), and dimethyl sulfoxide (DMSO, ε = 46.83).

The one-electron thermodynamic reduction potentials (E_{red}) are calculated by the following equation [59,60]:

$$E_{red}\left(Li/Li^+\right) = -\frac{\Delta G_{sol}}{F} - 1.46 \quad (1)$$

where ΔG_{sol} represents the Gibbs free energy of reduction in the solvated environment, F is the Faraday constant and 1.46 V is the absolute reduction electrode potential of Li/Li^+. The reaction free energies (ΔG) are calculated at 298 K. The average binding energies of explicit solvent molecules with Li^+ ($\overline{E_b}$) are calculated by the following equation:

$$\overline{E_b} = \frac{E_{tot} - [E_{Li+} + nE_{solvent}]}{n} \quad (2)$$

where E_{tot}, E_{Li+}, and $E_{solvent}$ are the computed free energies of the solvated lithium ion-solvent complex, the solvated lithium cation and the solvent molecules, respectively.

4. Conclusions

We perform computational investigations to quantify the influences of the DN and the ε of the solvent system to the relative stability of the polysulfide intermediates in Li-S batteries. The theoretical reduction mechanisms of the PSs under different solvation situations in different solvent systems are shown in Scheme 1. In general, the higher the DN and ε of the solvent, the more favorable the dissociated PS to the bound LiPS, and vice versa. Our theoretical calculations predict different major species when the reduction reactions proceed in the dissociated PS or the bound LiPS state. Our results confirm and rationalize the experimentally observed stability of S_6^{2-} and S_3^- in solvents with high DN and high ε, and the observed stability of Li_2S_8 and Li_2S_4 in solvents with low DN and low ε. For solvents with a high ε but a low DN, e.g., acetone, the two states shall exist in a chemical equilibrium and the dominant species will depend on the competing forces between solvation and coordination. We hope these results offer a clearer microscopic picture and will inspire the future optimization of the electrolyte systems.

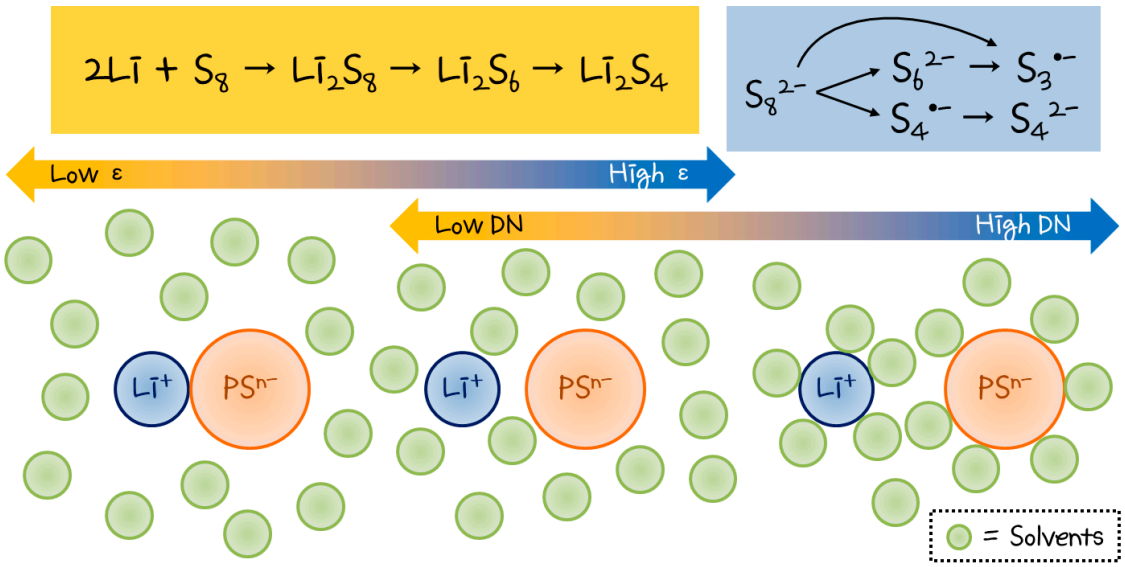

Scheme 1. Schematic presentation for the solvent interaction with the PS or LiPS species and the corresponding reduction reaction mechanisms in different solvent systems.

Supplementary Materials: The following are available online at http://www.mdpi.com/2073-4344/10/8/911/s1, Figure S1: Optimized geometries of (a) neutral, (b-d) singly-charged, and (e-i) doubly-charged polysulfides in DMSO. Figure S2: Optimized geometries of (a) [Li-(ACN)n]+ and (b) [Li-(DMSO)n]+ clusters with different solvent coordination numbers (n). Table S1: Theoretical values and the reported experimental results of reduction potentials (ΔE, in V) of S8, S82-, and S3•- in different solvents.

Author Contributions: G.-Y.D. performed the theoretical calculations; G.-Y.D. and C.-Y.L. wrote the manuscript draft; E.Y.L. supervised the research and revised the manuscript. All authors discussed together. All authors have read and agreed to the published version of the manuscript.

Funding: This research was funded by the Ministry of Science and Technology (MOST) in Taiwan (MOST 106-2113-M-003-010-MY3).

Conflicts of Interest: The authors declare no conflict of interest.

References

1. Yin, Y.-X.; Xin, S.; Guo, Y.-G.; Wan, L.-J. Lithium–sulfur batteries: Electrochemistry, materials, and prospects. *Angew. Chem. Int. Ed.* **2013**, *52*, 13186–13200. [CrossRef] [PubMed]
2. Ould Ely, T.; Kamzabek, D.; Chakraborty, D.; Doherty, M.F. Lithium-sulfur batteries: State of the art and future directions. *ACS Appl. Energy Mater.* **2018**, *1*, 1783–1814. [CrossRef]

3. Tarascon, J.-M.; Armand, M. Issues and challenges facing rechargeable lithium batteries. *Nature* **2001**, *414*, 359–367. [CrossRef] [PubMed]
4. Kang, W.; Deng, N.; Ju, J.; Li, Q.; Wu, D.; Ma, X.; Li, L.; Naebe, M.; Cheng, B. A review of recent developments in rechargeable lithium–sulfur batteries. *Nanoscale* **2016**, *8*, 16541–16588. [CrossRef] [PubMed]
5. Wild, M.; O'Neill, L.; Zhang, T.; Purkayastha, R.; Minton, G.; Marinescu, M.; Offer, G.J. Lithium sulfur batteries, a mechanistic review. *Energy Environ. Sci.* **2015**, *8*, 3477–3494. [CrossRef]
6. Eroglu, D.; Zavadil, K.R.; Gallagher, K.G. Critical link between materials chemistry and cell-level design for high energy density and low cost lithium-sulfur transportation battery. *J. Electrochem. Soc.* **2015**, *162*, A982. [CrossRef]
7. Hagen, M.; Hanselmann, D.; Ahlbrecht, K.; Maca, R.; Gerber, D.; Tubke, J. Lithium-sulfur cells: The gap between the state-of-the-art and the requirements for high energy battery cells. *Adv. Energy Mater.* **2015**, *5*, 1401986. [CrossRef]
8. Salama, M.; Rosy Attias, R.; Yemini, R.; Gofer, Y.; Aurbach, D.; Noked, M. Metal–sulfur batteries: Overview and research methods. *ACS Energy Lett.* **2019**, *4*, 436–446. [CrossRef]
9. Fang, R.; Zhao, S.; Sun, Z.; Wang, D.-W.; Cheng, H.-M.; Li, F. More reliable lithium-sulfur batteries: Status, solutions and prospects. *Adv. Mater.* **2017**, *29*, 1606823. [CrossRef]
10. Wang, H.; Sa, N.; He, M.; Liang, X.; Nazar, L.F.; Balasubramanian, M.; Gallagher, K.G.; Key, B. In situ NMR observation of the temporal speciation of lithium sulfur batteries during electrochemical cycling. *J. Phys. Chem. C* **2017**, *121*, 6011–6017. [CrossRef]
11. Busche, M.R.; Adelhelm, P.; Sommer, H.; Schneider, H.; Leitner, K.; Janek, J. Systematical electrochemical study on the parasitic shuttle-effect in lithium-sulfur-cells at different temperatures and different rates. *J. Power Sources* **2014**, *259*, 289–299. [CrossRef]
12. Xu, N.; Qian, T.; Liu, X.; Liu, J.; Chen, Y.; Yan, C. Greatly suppressed shuttle effect for improved lithium sulfur battery performance through short chain intermediates. *Nano Lett.* **2017**, *17*, 538–543. [CrossRef]
13. Lin, D.; Liu, Y.; Cui, Y. Reviving the lithium metal anode for high-energy batteries. *Nat. Nanotechnol.* **2017**, *12*, 194. [PubMed]
14. Bruce, P.G.; Freunberger, S.A.; Hardwick, L.J.; Tarascon, J.-M. Li–O2 and Li–S batteries with high energy storage. *Nat. Mater.* **2012**, *11*, 19. [CrossRef] [PubMed]
15. Carbone, L.; Coneglian, T.; Gobet, M.; Munoz, S.; Devany, M.; Greenbaum, S.; Hassoun, J. A simple approach for making a viable, safe, and high-performances lithium-sulfur battery. *J. Power Sources* **2018**, *377*, 26–35. [CrossRef]
16. Angulakshmi, N.; Stephan, A.M. Efficient electrolytes for lithium–sulfur batteries. *Front. Energy Res.* **2015**, *3*, 17. [CrossRef]
17. Younesi, R.; Veith, G.M.; Johansson, P.; Edstrom, K.; Vegge, T. Lithium salts for advanced lithium batteries: Li–metal, Li–O 2, and Li–S. *Energy Environ. Sci.* **2015**, *8*, 1905–1922. [CrossRef]
18. Xu, J.; Zhang, W.; Fan, H.; Cheng, F.; Su, D.; Wang, G. Promoting lithium polysulfide/sulfide redox kinetics by the catalyzing of zinc sulfide for high performance lithium-sulfur battery. *Nano Energy* **2018**, *51*, 73–82. [CrossRef]
19. Li, X.; Cao, Y.; Qi, W.; Saraf, L.V.; Xiao, J.; Nie, Z.; Mietek, J.; Zhang, J.-G.; Stchwenzer, B.; Liu, J. Optimization of mesoporous carbon structures for lithium–sulfur battery applications. *J. Mater. Chem.* **2011**, *21*, 16603–16610. [CrossRef]
20. Ghosh, A.; Garapati, M.S.; Saroja, A.P.V.K.; Sundara, R. Polar Bilayer Cathode for Advanced Lithium–Sulfur Battery: Synergy Between Polysulfide Conversion and Confinement. *J. Phys. Chem. C* **2019**, *123*, 10777–10787. [CrossRef]
21. Fang, X.; Peng, H. A revolution in electrodes: Recent progress in rechargeable lithium–sulfur batteries. *Small* **2015**, *11*, 1488–1511. [CrossRef] [PubMed]
22. Paolella, A.; Demers, H.; Chevallier, P.; Gagnon, C.; Girard, G.; Delaporte, N.; Zhu, W.; Vigh, A.; Guerfi, A.; Zaghib, K. A platinum nanolayer on lithium metal as an interfacial barrier to shuttle effect in Li-S batteries. *J. Power Sources* **2019**, *427*, 201–206. [CrossRef]
23. Paolella, A.; Laul, D.; Timoshevskii, V.; Zhu, W.; Marras, S.; Bertoni, G.; Wahba, A.S.; Girard, G.; Gagnon, C.; Rodrigue, L.; et al. The role of metal disulfide interlayer in Li–S batteries. *J. Phys. Chem. C* **2018**, *122*, 1014–1023. [CrossRef]

24. Liu, J.; HYuan, L.; Yuan, K.; Li, Z.; Hao, Z.; Xiang, J.; Huang, Y. SnO2 as a high-efficiency polysulfide trap in lithium–sulfur batteries. *Nanoscale* **2016**, *8*, 13638–13645. [CrossRef] [PubMed]
25. Wu, F.; Ye, Y.; Chen, R.; Qian, J.; Zhao, T.; Li, L.; Li, W. Systematic effect for an ultralong cycle lithium–sulfur battery. *Nano Lett.* **2015**, *15*, 7431–7439. [CrossRef] [PubMed]
26. Lochala, J.; Liu, D.; Wu, B.; Robinson, C.; Xiao, J. Research progress toward the practical applications of lithium–sulfur batteries. *ACS Appl. Mater. Inter.* **2017**, *9*, 24407–24421. [CrossRef]
27. Chen, X.; Hou, T.; Persson, K.A.; Zhang, Q. Combining theory and experiment in lithium–sulfur batteries: Current progress and future perspectives. *Mater. Today* **2019**, *22*, 142–158. [CrossRef]
28. Park, C.; Ronneburg, A.; Risse, S.; Ballauff, M.; Kanduc, M.; Dzubiella, J. Structural and Transport Properties of Li/S Battery Electrolytes: Role of the Polysulfide Species. *J. Phys. Chem. C* **2019**, *123*, 10167–10177. [CrossRef]
29. Kamphaus, E.P.; Balbuena, P.B. Long-chain polysulfide retention at the cathode of Li–S batteries. *J. Phys. Chem. C* **2016**, *120*, 4296–4305. [CrossRef]
30. Park, C.; Kanduc, M.; Chudoba, R.; Ronneburg, A.; Risse, S.; Ballauff, M.; Dzubiella, J. Molecular simulations of electrolyte structure and dynamics in lithium–sulfur battery solvents. *J. Power Sources* **2018**, *373*, 70–78. [CrossRef]
31. Camacho-Forero, L.E.; Smith, T.W.; Bertolini, S.; Balbuena, P.B. Reactivity at the lithium–metal anode surface of lithium–sulfur batteries. *J. Phys. Chem. C* **2015**, *119*, 26828–26839. [CrossRef]
32. Liu, Z.; Bertolini, S.; Balbuena, P.B.; Mukherjee, P.P. Li_2S film formation on lithium anode surface of Li–S batteries. *ACS Appl. Mater. Interfaces* **2016**, *8*, 4700–4708. [CrossRef] [PubMed]
33. Pascal, T.A.; Wujcik, K.H.; Velasco-Velez, J.; Wu, C.; Teran, A.A.; Kapilashrami, M.; Cabana, J.; Guo, J.; Salmeron, M.; Balsara, N.; et al. X-ray absorption spectra of dissolved polysulfides in lithium–sulfur batteries from first-principles. *J. Phys. Chem. Lett.* **2014**, *5*, 1547–1551. [CrossRef] [PubMed]
34. Kawase, A.; Shirai, S.; Yamoto, Y.; Arakawa, R.; Takata, T. Electrochemical reactions of lithium–sulfur batteries: An analytical study using the organic conversion technique. *Phys. Chem. Chem. Phys.* **2014**, *16*, 9344–9350. [CrossRef] [PubMed]
35. Lu, Y.-C.; He, Q.; Gasteiger, H.A. Probing the lithium–sulfur redox reactions: A rotating-ring disk electrode study. *J. Phys. Chem. C* **2014**, *118*, 5733–5741. [CrossRef]
36. Assary, R.S.; Curtiss, L.A.; Moore, J.S. Toward a molecular understanding of energetics in Li–S batteries using nonaqueous electrolytes: A high-level quantum chemical study. *J. Phys. Chem. C* **2014**, *118*, 11545–11558. [CrossRef]
37. See, K.A.; Wu, H.-L.; Lau, K.C.; Shin, M.; Cheng, L.; Balasubramanian, M.; Gallagher, K.G.; Curtiss, L.A.; Gewirth, A.A. Effect of hydrofluoroether cosolvent addition on Li solvation in acetonitrile-based solvate electrolytes and its influence on S reduction in a Li–S battery. *ACS Appl. Mater. Interfaces* **2016**, *8*, 34360–34371. [CrossRef]
38. Zou, Q.; Lu, Y.-C. Solvent-dictated lithium sulfur redox reactions: An operando UV–vis spectroscopic study. *J Phys. Chem. Lett.* **2016**, *7*, 1518–1525. [CrossRef]
39. Pascal, T.A.; Wujcik, K.H.; Wang, D.R.; Balsara, N.P.; Prendergast, D. Thermodynamic origins of the solvent-dependent stability of lithium polysulfides from first principles. *Phys. Chem. Chem. Phys.* **2017**, *19*, 1441–1448. [CrossRef]
40. Wu, H.-L.; Huff, L.A.; Gewirth, A.A. In situ Raman spectroscopy of sulfur speciation in lithium–sulfur batteries. *ACS Appl. Mater. Interfaces* **2015**, *7*, 1709–1719. [CrossRef]
41. Vijayakumar, M.; Govind, N.; Walter, E.; Burton, S.D.; Shukla, A.; Devaraj, A.; Xiao, J.; Liu, J.; Wang, C.; Karim, A.; et al. Molecular structure and stability of dissolved lithium polysulfide species. *Phys. Chem. Chem. Phys.* **2014**, *16*, 10923–10932. [CrossRef] [PubMed]
42. Cheng, L.; Curtiss, L.A.; Zavadil, K.R.; Gewirth, A.A.; Shao, Y.; Gallagher, K.G. Sparingly solvating electrolytes for high energy density lithium–sulfur batteries. *ACS Energy Lett.* **2016**, *1*, 503–509. [CrossRef]
43. Wujcik, K.H.; Wang, D.R.; Raghunathan, A.; Drake, M.; Pascal, T.A.; Prendergast, D.; Balsara, N.P. Lithium polysulfide radical anions in ether-based solvents. *J. Phys. Chem. C* **2016**, *120*, 18403–18410. [CrossRef]
44. Steudel, R.; Chivers, T. The role of polysulfide dianions and radical anions in the chemical, physical and biological sciences, including sulfur-based batteries. *Chem. Soc. Rev.* **2019**, *48*, 3279–3319. [CrossRef] [PubMed]

45. Cuisinier, M.; Hart, C.; Balasubramanian, M.; Garsuch, A.; Nazar, L.F. Radical or not radical: Revisiting lithium–sulfur electrochemistry in nonaqueous electrolytes. *Adv. Energy Mater.* **2015**, *5*, 1401801. [CrossRef]
46. Zou, Q.; Liang, Z.; Du, G.-Y.; Liu, C.-Y.; Li, E.Y.; Lu, Y.-C. Cation-directed selective polysulfide stabilization in alkali metal–sulfur batteries. *J. Am. Chem. Soc.* **2018**, *140*, 10740–10748. [CrossRef]
47. Li, G.; Li, Z.; Zhang, B.; Lin, Z. Developments of electrolyte systems for lithium–sulfur batteries: A review. *Front. Energy Res.* **2015**, *3*, 5. [CrossRef]
48. Wujcik, K.H.; Pascal, T.A.; Pemmaraju, C.D.; Devaux, D.; Stolte, W.C.; Balsara, N.P.; Prendergast, D. Characterization of Polysulfide Radicals Present in an Ether-Based Electrolyte of a Lithium–Sulfur Battery During Initial Discharge Using In Situ X-Ray Absorption Spectroscopy Experiments and First-Principles Calculations. *Adv. Energy Mater* **2015**, *5*, 1500285. [CrossRef]
49. Wang, B.; Alhassan, S.M.; Pantelides, S.T. Formation of large polysulfide complexes during the lithium-sulfur battery discharge. *Phys. Rev. Appl.* **2014**, *2*, 034004. [CrossRef]
50. Xin, S.; Gu, L.; Zhao, N.-H.; Yin, Y.-X.; Zhou, L.-J.; Guo, Y.-G.; Wan, L.-J. Smaller sulfur molecules promise better lithium–sulfur batteries. *J. Am. Chem. Soc.* **2012**, *134*, 18510–18513. [CrossRef]
51. Steudel, R.; Steudel, Y. Polysulfide Chemistry in Sodium-Sulfur Batteries and Related Systems–A Computational Study by G3X (MP2) and PCM Calculations. *Chem.: Eur. J.* **2013**, *19*, 3162–3176. [CrossRef] [PubMed]
52. Patel, M.U.M.; Dominko, R. Application of in operando UV/vis spectroscopy in lithium–sulfur batteries. *ChemSusChem* **2014**, *7*, 2167–2175. [CrossRef] [PubMed]
53. Patel, M.U.M.; Demir-Cakan, R.; Morcrette, M.; Tarascon, J.-M.; Gaberscek, M.; Dominko, R. Li-S Battery Analyzed by UV/Vis in Operando Mode. *ChemSusChem* **2013**, *6*, 1177–1181. [CrossRef] [PubMed]
54. Fawcett, W.R. Acidity and basicity scales for polar solvents. *J. Phys. Chem.* **1993**, *97*, 9540–9546. [CrossRef]
55. He, Q.; Gorlin, Y.; Patel, M.U.; Gasteiger, H.A.; Lu, Y.-C. Unraveling the correlation between solvent properties and sulfur redox behavior in lithium-sulfur batteries. *J. Electrochem. Soc.* **2018**, *165*, A4027. [CrossRef]
56. Frisch, M.J.; Trucks, G.W.; Schlegel, H.B.; Scuseria, G.E.; Robb, M.A.; Cheeseman, J.R.; Scalmani, G.; Barone, V.; Petersson, G.A.; Nakatsuji, H.; et al. *Gaussian 09*; Gaussian, Inc.: Wallingford, CT, USA, 2016.
57. Peverati, R.; Truhlar, D.G. Improving the accuracy of hybrid meta-GGA density functionals by range separation. *J. Phys. Chem. Lett.* **2011**, *2*, 2810–2817. [CrossRef]
58. Marenich, A.V.; Cramer, C.J.; Truhlar, D.G. Universal solvation model based on solute electron density and on a continuum model of the solvent defined by the bulk dielectric constant and atomic surface tensions. *J. Phys. Chem. B* **2009**, *113*, 6378–6396. [CrossRef]
59. Sriana, T.; Leggesse, E.G.; Jiang, J.C. Novel benzimidazole salts for lithium ion battery electrolytes: Effects of substituents. *Phys. Chem. Chem. Phys.* **2015**, *17*, 16462–16468. [CrossRef]
60. Marenich, A.V.; Ho, J.; Coote, M.L.; Cramer, C.J.; Truhlar, D.G. Computational electrochemistry: Prediction of liquid-phase reduction potentials. *Phys. Chem. Chem. Phys.* **2014**, *16*, 15068–15106. [CrossRef]

© 2020 by the authors. Licensee MDPI, Basel, Switzerland. This article is an open access article distributed under the terms and conditions of the Creative Commons Attribution (CC BY) license (http://creativecommons.org/licenses/by/4.0/).